Hydrogen Production in a Sorption-Enhanced Fluidized-Bed Membrane Reactor: Operating Parameter Investigation

ARTICLE *in* INDUSTRIAL & ENGINEERING CHEMISTRY RESEARCH · MARCH 2014

Impact Factor: 2.59 · DOI: 10.1021/ie500294k

7 AUTHORS, INCLUDING:

Yumin Chen
Huazhong University of Science and Technol…
4 PUBLICATIONS **16** CITATIONS
SEE PROFILE

Junying Zhang
Huazhong University of Science and Technol…
57 PUBLICATIONS **895** CITATIONS
SEE PROFILE

Yongchun Zhao
Huazhong University of Science and Technol…
68 PUBLICATIONS **407** CITATIONS
SEE PROFILE

I&EC research
Industrial & Engineering Chemistry Research

Article

pubs.acs.org/IECR

Hydrogen Production in a Sorption-Enhanced Fluidized-Bed Membrane Reactor: Operating Parameter Investigation

Yumin Chen,[†,‡] Andrés Mahecha-Botero,[§] C. Jim Lim,[‡] John R. Grace,[‡] Junying Zhang,*[,†] Yongchun Zhao,[†] and Chuguang Zheng[†]

[†]State Key Laboratory of Coal Combustion, Huazhong University of Science and Technology, Wuhan 430074, Hubei Province, People's Republic of China

[‡]Department of Chemical and Biological Engineering, University of British Columbia, 2360 East Mall, Vancouver, Canada V6T IZ3

[§]Noram Engineering and Constructors, 200 Granville Street, Suite 1800, Vancouver, Canada V6C 1S4

ABSTRACT: Sorption-enhanced steam reforming, assisted by membrane separation of H_2 in a fluidized bed reactor, is simulated numerically based on a kinetic two-phase model. A residence time distribution function method is implemented to account for CO_2 capture in continuous operation. The effects of operating pressure, total gas feed rate, solid recycle rate, fresh sorbent feed rate, effective membrane area, and permeate pressure on the performance of a continuous fluidized bed reactor are investigated. A CH_4 conversion of >91% for operation at 0.6 MPa and 550 °C is predicted to be possible with the assistance of the sorbent and membranes. The reforming performance is very sensitive to the effective surface area of membranes. A sorbent fraction of >0.7 (by mass) is necessary to achieve a product with H_2 selectivity of >98%, free of CO and CO_2, for realistic membrane effectiveness factors. Adding fresh sorbent or increasing the sorbent mass fraction improves the H_2 productivity for a moderate solids recycling rate. Effective CO_2 capture rate depends greatly on the sorbent feed rate.

1. INTRODUCTION

Steam methane reforming (SMR) is widely used in industry for the production of hydrogen from natural gas and water. However, this process emits CO_2, and it must be operated under severe conditions (800−900 °C, 1.5−3.0 MPa) to achieve high conversion of CH_4.[1] Furthermore, conventional SMR requires a purification step to provide CO-free gas for proton exchange membrane (PEM) fuel cells and other purposes.[2] Improvements in SMR to overcome these problems have received recent attention.[3] Fluidized-bed reactors facilitate efficient heat transfer, temperature uniformity, low pressure drop, and high catalyst effectiveness factors.[4] Sorption-enhanced steam methane reforming (SE-SMR) has been proposed as a means of integrating standard SMR with in situ CO_2 capture.[5] With the removal of CO_2 from the gas phase, the thermodynamic equilibrium is shifted to the product side,[6] increasing the CH_4 conversion, even if operation is at a temperature lower than that for conversional SMR.

SE-SMR has been studied in experiments[7−11] and simulations,[12,13] exhibiting very good H_2 selectivity and enhanced CH_4 conversion. Production of >90% H_2 and near-zero CO concentration can be obtained at temperatures <550 °C.[9] CH_4 conversion enhancement of 78% can be achieved at 450 °C in a fixed-bed reactor.[10] Johnsen et al.[14] found that the concentration of hydrogen on a dry basis remained 98−99% after four reforming/calcination cycles in a SE-SMR experiment conducted at atmospheric pressure with dolomite as a CO_2 sorbent in a fluidized-bed reactor.

Numerical studies of SE-SMR in a fluidized-bed reactor have also been carried out. Carlo et al.[15] investigated the SE-SMR process with dolomite as a CO_2 acceptor in a fluidized bed, based on an Eulerian−Eulerian CFD model. Wang et al.[16,17] studied SE-SMR with sorbent regeneration and CaO as sorbent in bubbling fluidized-bed reactors. It was found that the sorption kinetics of the adsorbent and the operating pressure profoundly affected the production efficiency. Increasing the operating pressure led to decreased CH_4 conversion, even with a sorbent present,[12,16,17] consistent with Le Chatelier's principle and the overall reaction

$$CH_4 + 2H_2O + CaO \Leftrightarrow CaCO_3 + 4H_2 \quad (1)$$

However, high-pressure operating conditions are attractive for improving the throughput for a given reactor.

The conversion of CH_4 can also be enhanced by selective separation of H_2 via membranes.[18,19] The rate of H_2 permeation through a palladium or palladium alloy membrane[20] is written as

$$Q_{H_2,p} = A_p \frac{P_{M0}}{\delta_{H_2}} \exp\left(-\frac{E_{H_2}}{RT}\right)\left(\sqrt{P_{H_2}} - \sqrt{P_{H_2,p}}\right) \quad (2)$$

Equation 2 shows that the permeation can be increased by increasing the partial pressure of H_2 (P_{H_2}) inside the reactor and/or decreasing the partial pressure of H_2 ($P_{H_2,p}$) inside the membranes (i.e., by using vacuum or gas sweeping). Membrane separation of H_2 can help to maximize the conversion of hydrocarbons under high pressure operating conditions for steam reforming. Rakib et al.[21,22] conducted steam reforming experiments with heptane and propane as feedstocks in a fluidized-bed membrane reactor (FBMR) at pressures of 0.4−0.6 MPa. Hydrogen purities exceeding 99.99% were obtained by

Received: January 21, 2014
Revised: March 6, 2014
Accepted: March 11, 2014

   dx.doi.org/10.1021/ie500294k | *Ind. Eng. Chem. Res.* XXXX, XXX, XXX−XXX

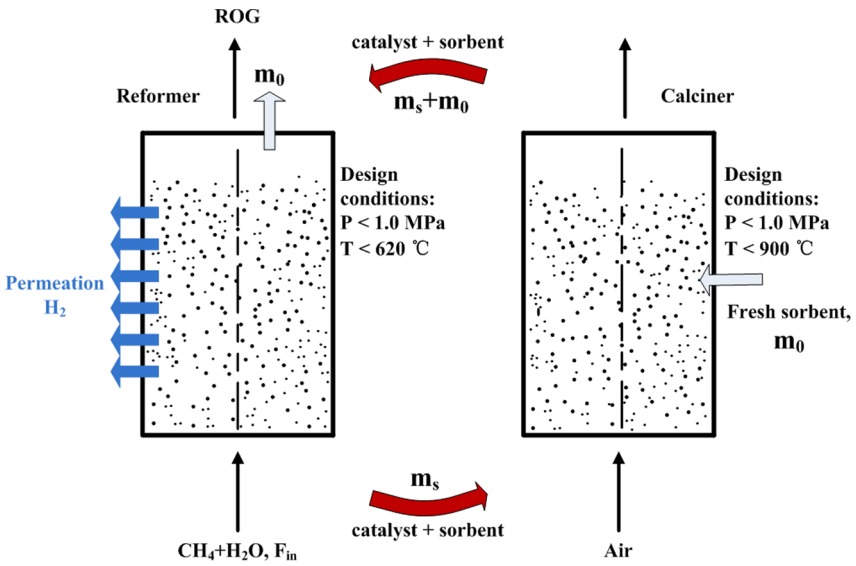

Figure 1. Schematic of an integrated reformer/calciner system.

Table 1. Balance Equations

mass balance, L-phase

$$\frac{1}{A}\vec{\nabla}\cdot[N_{i_L}] = \psi_L\sum_{\substack{n=1\\n\neq L}}^{N_L}\alpha_{I_{(H\to L)}}\kappa_{C_{i,(H\to L)}}(C_i - C_{iL}) - \psi_L\sum_{\substack{n=1\\n\neq L}}^{N_L}Q_{bulk_{(L\to H)}}(C_{iL}) + \psi_H\sum_{\substack{n=1\\n\neq H}}^{N_H}Q_{bulk_{(H\to L)}}(C_{iH}) + [\psi_L(1-\varepsilon_L)\alpha_{cat}\rho_s\sum_{j=1}^{N_{R_{cat}}}r_{j_{cat,L}}a_{j_{cat,L}}] + \psi_L(1-\varepsilon_L)\alpha_{ads}\rho_s\sum_{j=1}^{N_{R_{sorb}}}r_{j_{cap,L}}a_{j_{sorb,L}} + [\psi_L\sum_{i=1}^{N_P}\beta A_{p,i}J_{i,L}]$$

mass balance, H-phase

$$\frac{1}{A}\vec{\nabla}\cdot[F_{i_L}] = \psi_H\sum_{\substack{n=1\\n\neq L}}^{N_L}\alpha_{I_{(L\to H)}}\kappa_{C_{i,(L\to H)}}(C_{iL} - C_{iH}) - \psi_H\sum_{\substack{n=1\\n\neq L}}^{N_L}Q_{bulk_{(H\to L)}}(C_{iH}) + \psi_L\sum_{\substack{n=1\\n\neq H}}^{N_H}Q_{bulk_{(L\to H)}}(C_{iL}) + \left[\psi_H(1-\varepsilon_H)\alpha_{cat}\rho_s\sum_{N_{R_{cat}}}^{j=1}r_{j_{cat,H}}a_{j_{cat,H}}\right] + \psi_H(1-\varepsilon_H)\alpha_{ads}\rho_s\sum_{j=1}^{N_{R_{sorb}}}r_{j_{cap,H}}a_{j_{sorb,H}} + \left[\psi_H\sum_{i=1}^{N_P}\beta A_{p,i}J_{i,H}\right]$$

pressure balance

$$-\frac{dP_L}{dz} = [(1-\varepsilon_T)\alpha_{cat}\rho_s g] + [(1-\varepsilon_L)\alpha_{ads}\rho_s g] + [\varepsilon_T\rho_{gas}g]$$

H_2 permeate equation

$$\frac{d}{dz}(v_M C_{iM}) = \psi_L\beta A_{p,i}J_{i,L} + \psi_H\beta A_{p,i}J_{i,H}$$

Mahecha-Botero et al.[23,24] through membrane separation, with two different natural gas feedstocks. Steam reforming in FBMRs has also been studied based on different reactor models, including an equilibrium model,[19,25] kinetic two-phase model[26,27] and a comprehensive kinetic model.[28−30]

While all previous experiments confirm that the conversion of hydrocarbon can be augmented by permselective membranes, full conversion of CH_4 is difficult to achieve because of limited membrane permeation. To maximize the conversion of feedstock (methane, heptane, propane, etc.) and obtain near-zero carbon products in a single unit at moderate operating temperatures and elevated pressures, a novel steam reforming process was proposed,[19] combining sorption-enhancement and membrane separation in a single fluidized-bed reactor. This process, denoted as MA-SE-SMR, was demonstrated to be feasible experimentally,[31] providing a product with H_2 fraction exceeding 99.99% in the permeate stream and almost no CO_2 and CO in the retentate for an operating pressure of 0.3 MPa. Investigation of the operating conditions is required to optimize the reforming efficiency. Properties of the sorbent and membrane also affect the synergistic enhancement greatly. However, reported works have yet to provide systemic analysis of MA-SE-SMR in fluidized-bed reactors.

In this paper, a one-dimensional (1-D), isothermal, simplified comprehensive kinetic model is used to simulate sorption-enhanced steam methane reforming assisted by membrane separation in a fluidized-bed reactor. The objective is to determine the dependence of reforming efficiency on the operating parameters and kinetic processes, including CO_2 capture and membrane permeation in a continuous fluidized-bed reformer. Model verification is performed in the first part of this work. In the second part, special attention is focused on investigating the effect of operating pressure, total gas feed rate, in-bed sorbent mass fraction, sorbent recycle rate, and fresh sorbent feed rate on the reforming performance. The sensitivities of CH_4 conversion, CO_2 production, and CO generation to the H_2 permeation rate and CO_2 sorption rate are also analyzed.

dx.doi.org/10.1021/ie500294k | Ind. Eng. Chem. Res. XXXX, XXX, XXX−XXX

2. REACTOR MODEL

2.1. Conservation Equations. Figure 1 presents a schematic of the integrated reformer/calciner system, and further details can be found elsewhere.[21,22] Each gas-fluidized bed is considered to be composed of two distinct phases, a high-density (emulsion) phase and a low-density (dilute) phase,[32,33] which is a widely accepted practice in modeling gas−solid fluidized-bed reactors.[34,35] Adris et al.[36] applied a two-phase model in modeling steam methane reforming in FBMRs, taking membrane separation into consideration. A generic model, covering three different fluidization flow regimes—bubbling, turbulent, and fast fluidization[37]—was applied to simulate autothermal steam methane reforming[38] and steam methane reforming[29,30] in a FBMR, gave satisfactory results.

The generic model integrating H_2 separation and CO_2 capture is employed in this study. The mass balance equations for the two phases and the average pressure balance equation are listed in Table 1. Compared with eq 2, a membrane effectiveness factor (β) is employed in terms describing H_2 permeate flux in the mass balance equations in Table 1. In a fluidized-bed reformer, the active membrane area (A_p, relative to the ideal permeate area, usually taken as the geometric area of the membrane) would be reduced by the blockage/coverage of particles, and interphase mass-transfer limitations also slow the external diffusion of H_2 to the membrane wall. β accounts for the decrease of membrane permeability in a fluidized bed from the ideal permeability calculated by eq 2. Hydrodynamic parameters are given in Table 2. Several key model assumptions are specified as follows:

Table 2. Hydrodynamic Parameters for the Fluidized-Bed Model

parameter	equation	ref(s)
minimum fluidization velocity, U_{mf}	$U_{mf} = \left(\frac{\mu_g}{d_p\rho_g}\right)(27.2^2 + 0.0408Ar^{1/2} - 27.2)$	39, 40
bubble velocity, U_b	$U_b = Y(U - U_{mf}) + 0.711(gd_b)^{1/2}$	41
bubble diameter, d_b	$d_b = 0.54(U - U_{mf})^{0.4}\left(h + 4\sqrt{\frac{A}{N_{or}}}\right)^{0.8} g^{-0.2}$	42
maximum bubble size, d_{bm}	$d_{bm} = 1.64[A(U - U_{mf})]^{0.4}$	43
volume fraction occupied by bubbles, ε_b	$\varepsilon_b = 1 - \left[\frac{1 - \varepsilon_{mf}}{\left(1 + \frac{U - U_{mf}}{0.711\sqrt{gd_b}}\right)}\right]$	44
mass exchange coefficient, k_{iq}	$k_{iq} = \frac{U_{mf}}{3} + \left[\frac{4D_{ie}\varepsilon_{mf}U_b}{\pi d_b}\right]^{0.5}$, species i	41
effective diffusivity, D_{ie}	$\frac{(1 - y_i)}{D_{ie}} = \sum_{n}^{i=1}\left(\frac{y_i}{D_{ij}}\right)$	45
binary diffusion coefficient, D_{ij}	$D_{ij} = 0.001888\frac{\left[T^3\left(\frac{1}{M_{w,i}} + \frac{1}{M_{w,j}}\right)\right]^{0.5}}{P_{abs}\sigma_{ij}^2\Omega_D}$	46
hydrogen flux (membrane), J	$J = \frac{P_{M0}}{\delta_{H_2}}\exp\left(\frac{E_{H_2}}{RT}\right)\left(\sqrt{P_{H_2}} - \sqrt{P_{H_2,P}}\right)$	20

- *Pseudo-phases:* A high-density (emulsion) phase and low-density (dilute) phase are considered. The gas in both phases is treated as being in plug flow, with mass exchange between phases. Mole and energy balance equations are imposed on both phases.
- *Particle properties:* Catalyst and sorbent particles are assumed to have similar physical properties so that segregation is neglected. Changes in particle density and diameter due to carbon deposition, CO_2 adsorption, and particle breakage are also neglected.
- *Chemical reactions:* Species generation and consumption take place in both phases. Intraparticle diffusion resistances are neglected for catalytic reactions. The solid volume fraction in the low-density phase is assumed to be 0.1%.[48] A constant solid volume fraction in the high-density phase equal to ε_{mf} is assumed. So, the void fraction of the low- and high-density phase are

$$\varepsilon_L = 0.999 \tag{3}$$

$$\varepsilon_H = \varepsilon_{mf} \tag{4}$$

- *Temperature:* The particle temperature is identical to the local gas temperature.
- *Gas properties:* All gas species are treated as ideal gases. So, the molar concentration of species i in phase φ (φ = H,L) at a given height above the distributor is

$$C_{i_\varphi} = \frac{F_{i_L}}{\upsilon_\varphi} \tag{5}$$

with a total volumetric flow rate given by

$$\upsilon_\varphi = \frac{RT_\varphi}{P}\sum_{i=1}^{N_\varphi} F_{i_\varphi} \tag{6}$$

The gas superficial velocity in each phase is expressed as

$$U_{gas_\varphi} = \frac{\upsilon_\varphi}{A\psi_\varphi\varepsilon_\varphi} \tag{7}$$

The bed superficial velocity used in the calculations is given by

$$U = \frac{\upsilon_L + \upsilon_H}{A} \tag{8}$$

At the inlet of the reactor,

$$F_{CH_4,in} = \frac{P_{in}\mathrm{Feed}_{CH_4,in}}{RT_{in}} \tag{9}$$

where $\mathrm{Feed}_{CH_4,in}$ and $F_{CH_4,in}$ are the volumetric and molar feed rates of methane, respectively.

- *Interphase diffusional mass transfer:* Interphase species transport between the H-phase and the L-phase results from differences in species concentrations in the two phases. The interphase mass transfer is estimated by the equation of Sit and Grace,[41] as indicated in Table 2.
- *Balancing cross-flow mass transfer:* Bulk mass exchange between the phases is considered, with the direction depending on the fluidization conditions. When the flow rate is less than required for minimum fluidization due to H_2 permeation, CO_2 capture, and/or changes in temperature or pressure, gas is assumed to migrate between the H-phase and the L-phase to avoid defluidization. The species composition of the bulk transfer flow is the same as that of the local source phase. The flow requirement in the high-density phase at a given height is

$$Q_{H,req} = U_{mf}(1 - \psi_L)A \tag{10}$$

The volumetric exchange terms are written as

(a) if $\upsilon_H > Q_{H,req}$, excess gas flows from the H-phase to the L-phase,

dx.doi.org/10.1021/ie500294k | Ind. Eng. Chem. Res. XXXX, XXX, XXX−XXX

Table 3. Reaction Rate Equations for SMR

	reaction	rate equation and kinetic parameters	enthalpy (ΔH_{298})	ref
1.	$CH_4 + H_2O \Leftrightarrow CO + 3H_2$	$r_1 = \frac{k_1}{P_{H_2}^{2.5}}\left[\frac{P_{CH_4}P_{H_2O} - P_{H_2}^3 P_{CO}/K_1}{DEN^2}\right]$	206.2×10^3 J/mol	47
2.	$CH_4 + 2H_2O \Leftrightarrow CO_2 + 4H_2$	$r_2 = \frac{k_2}{P_{H_2}^{3.5}}\left[\frac{P_{CH_4}P_{H_2O}^2 - P_{H_2}^4 P_{CO_2}/K_2}{DEN^2}\right]$	164.9×10^3 J/mol	47
3.	$CO + H_2O \Leftrightarrow CO_2 + H_2$	$r_3 = \frac{k_3}{P_{H_2}}\left[\frac{P_{CO}P_{H_2O} - P_{H_2}P_{CO_2}/K_3}{DEN^2}\right]$	-41.1×10^3 J/mol	47
4.	$CaO + CO_2 \Leftrightarrow CaCO_3$	$\frac{dX}{dt} = \frac{\left(\frac{3}{R_p}\right)(1-X)^{2/3}\frac{1}{\rho_{m,CaO}RT}(P_{CO_2} - P_{CO_2,eq})^n}{\frac{1}{k_{cap}} + \frac{R_p[(1-X)^{1/3} - (1-X)^{2/3}]}{D_e} + \frac{(1-X)^{2/3}}{k_g}}$	-178.8×10^3 J/mol	4

where

$$DEN = 1 + K_{CO}P_{CO} + K_{H_2}P_{H_2} + K_{CH_4}P_{H_2} + K_{H_2O}\left(\frac{P_{H_2O}}{P_{H_2}}\right)$$

$$Q_{H\to L} = \upsilon_H - Q_{H,req}$$

$$Q_{L\to H} = 0$$

(b) if $\upsilon_H < Q_{H,req}$, gas flows to the H-phase to avoid defluidization,

$$Q_{L\to H} = Q_{H,req} - \upsilon_H$$

$$Q_{H\to L} = 0$$

• *Fluidization flow regime:* The flow regime is mainly bubbling fluidization.[37] However, the slugging flow regime can also be considered.

• *Freeboard:* The temperature drop in the freeboard leads to the reverse reaction, which affects the ultimate conversion, to a certain extent.[21−23] We assume the solid volumetric concentration to be 0.1% in the freeboard region.

• *Gas flow modification factor:* An adjustable factor Y is used to account for deviations between bubble phase gas flow and the predication of the simple two-phase theory.[44,49] According to the dimensional correlation proposed by Peter et al.,[50] $Y = 0.7585 - 0.13(U - U_{mf}) + 5(U - U_{mf})^2$, $Y = 0.8$ is assumed for the particles in this work. The feed gas splits into two streams going to the H-phase and the L-phase at the inlet. The inlet volumetric flow rates to the H-phase and the L-phase are then

$$Q_{L,in} = YA(U - U_{mf})_{in} \tag{11}$$

$$Q_{H,in} = AU_{in} - Q_{L,in} \tag{12}$$

2.2. Sorbent Conversion. The conversion profile of sorbent in the reactor is required to calculate the CO_2 capture rate. Several approaches are provided to estimate the sorbent conversion. Here, we consider the continuous bed, in which the sorbent adsorbs CO_2 in the reformer and is regenerated in the calciner, then re-enters the reformer, as shown in Figure 1. Several assumptions are specified:

(1) Perfect mixing: The mixing time of solids is significantly less than the mean residence time in both the reformer and the regenerator. As a result, the sorbent composition is approximated as being uniform in both reactors. Complete regeneration is achieved before the sorbent is returned to the reformer.

(2) Steady state: Both fluidized-bed reactors are assumed to have reached steady state.

(3) Characteristic time: Reaction rate is taken as zero after a characteristic time t^*. Here, the maximum conversion (X_N) is taken as the cumulative conversion at the end of the fast carbonation stage (i.e., the chemically controlled stage). For a spherical particle of diameter d_p, based on the shrinking-core model[4] and chemical-control assumption, t^* is written as

$$t^* = \frac{\rho_{m,cao}R_g T d_p}{2k_{cap}(P_{CO_2} - P_{eq})} \tag{13}$$

(4) Deactivation and regeneration of the catalyst: Deactivation and regeneration of the catalyst are beyond the scope of this study. The catalyst is recycled along with the sorbents, without being separated. Therefore, the molar sorbent recycling rate and fresh sorbent feed rate are written as

$$F_R = \frac{m_s \alpha_{ads}}{MW_{ads}} \tag{14}$$

$$F_0 = \frac{m_0}{MW_{ads}} \tag{15}$$

Since particles spend different times in the reactor simultaneously, they achieve different CO_2 capture. Particles that remain in the bed longer than time t^* fail to capture any more CO_2. Based on the perfect mixing assumption, the residence time distribution of reactive particles in the bed is calculated by

$$E(t) = \frac{1}{\bar{t}}\exp\left(-\frac{t}{\bar{t}}\right) \tag{16}$$

Integrating eq 14 from 0 to t^*, we obtain the reactive particle fraction in the bed:

$$f_a = F(E) = \int_0^{t^*} E(t)\,dt = \int_0^{t^*} \frac{1}{\bar{t}}\exp\left(-\frac{t}{\bar{t}}\right)dt = 1 - \exp\left(-\frac{t^*}{\bar{t}}\right) \tag{17}$$

where the average residence time ($\bar{t}$) is given by

$$\bar{t} = \frac{m_{bed,ad}}{F_R} \tag{18}$$

and $m_{bed,ad}$ is the initial loading of sorbent (in moles). To calculate the capture rate based on the kinetic equation shown in Table 3, the sorbent conversion (X), representing the fraction of $CaCO_3$ in reactive particles at the beginning of every calculation

dx.doi.org/10.1021/ie500294k | Ind. Eng. Chem. Res. XXXX, XXX, XXX−XXX

step, is required. If we assume that the conversion rate during time interval 0 to t^* is constant, the conversion of particles with a residence time t can be estimated by

$$X_{t(t<t*)} = \frac{X_{ave}}{t^*} \times t \times \frac{1}{\bar{t}} \exp\left(-\frac{t}{\bar{t}}\right) \tag{19}$$

Therefore, the conversion (X) can be derived by integrating eq 19 from time 0 to t^*:

$$X = X_{t<t^*} = \frac{\int_0^{t^*} \left(\frac{X_{ave}}{t} \times t\right)\frac{1}{\bar{t}} \exp\left(-\frac{t}{\bar{t}}\right) dt}{f_a} = X_{ave}\frac{\left[1 - \exp\left(-\frac{t^*}{\bar{t}}\right)\left(\frac{t^*}{\bar{t}} + 1\right)\right]}{f_a} \tag{20}$$

For particles with residence times longer than t^*, the conversion equals the population average of ultimate conversion for N cycles,[51]

$$X_{ave} = \sum_{N=1}^{\infty} r_N X_N \tag{21}$$

where r_N is the mass fraction of particles, which have circulated N times, in the solids stream ($F_0 + F_R$) entering the reformer, calculated[51] from

$$r_N = \frac{F_0 F_R{}^{N-1}}{(F_0 + F_R)^N} \tag{22}$$

The maximum conversion (X_N) is calculated using an equation of the following form:[52]

$$X_N = f^{N+1} + b \tag{23}$$

The overall carbon balance in the system[53] can be written as

(moles of carbon removed from gas phase)
= (moles of $CaCO_3$ formed in sorbent outlet stream)
= (moles of CO_2 reacting with active CaO in bed)

Given perfect solids mixing in the reformer, we can estimate the sorbent conversion in the outlet stream, which can be calculated based on the carbon balance:

$$X_{ex} = \frac{(CO_2 \text{ reacting with active CaO in bed})}{F_0 + F_R} = \frac{\int_{z=0}^{z=H_{max}} (r_{cap,H} + r_{cap,L})\, dz}{F_0 + F_R} \tag{24}$$

where $r_{cap,\varphi}$ (φ = H, L) is the CO_2 capture rate at height z above the distributor. The parameter $r_{cap,\varphi}$ can be estimated from the CO_2 capture kinetic model in Table 3. Since, within times less than t^*, the reaction rate is chemically controlled, a simplified model can be utilized:

$$r_{cap,\varphi}\ (\text{mol/m}^3\ \text{s}) = f_a X_N \psi_\varphi (1 - \varepsilon_\varphi)\left(k_{cap}\frac{3}{R_p}\frac{1}{RT}(P_{CO_2} - P_{CO_{2,eq}})^n\right), \quad n = 1 \tag{25}$$

2.3. Computation Solution Strategy. For the computations, the one-dimensional (1D) FBMR is divided into 4720 sections with a mesh resolution of 0.5 mm. Conservation equations imposed on each subsection are solved by the Partial Differential Equation model in COMSOL Multiphysics 3.5a. The adaptive nonlinear solver is employed to reduce the iterations needed to achieve convergence, with a Dirichelet boundary condition and Neumann boundary condition imposed on the inlet and outlet, respectively, for the pressure and species, as shown by eqs 26 and 27.

$z = 0$:

$$F_{i,\varphi}\Big|_{z=0} = \frac{4P_{in}\text{Feed}_{CH_4,\varphi,in}}{RT_{in}} x_{in,i} \quad (i = CH_4, H_2O, CO_2, CO, H_2;\ \varphi = H, L)$$
$$P|_{z=0} = P_{in} \tag{26}$$

$z = L_0$:

$$\frac{\partial F_{i,\varphi}}{\partial z}\Big|_{z=L_0} = 0 \quad (i = CH_4, H_2O, CO_2, CO, H_2;\ \varphi = H, L)$$
$$\frac{\partial P}{\partial z}\Big|_{z=L_0} = 0 \tag{27}$$

The mesh independence has been checked by varying the mesh resolutions (1.0, 0.5, 0.35, 0.25 mm) in the calculations. Stable results are obtained after a mesh resolution ≤0.0005 m is employed. A constant temperature is assumed in the simulations, except when comparing modeling results with the experiment; in that case, a temperature profile fitted to experimentally recorded values[31] is used.

3. RESULTS AND DISCUSSION

3.1. Comparison of Predictions with Experimental Data. Values of the parameters used in this study for calculation purposes are listed in Table 4, and the kinetic and thermal dynamic data for the reactions involved are given in Table 5. To determine whether the model is capable of giving reasonable predictions for the MA-SE-SMR process, the simulation results and experimental data[31] are compared in this section. Calculations were started from a uniform sorbent conversion (X), which is the same assumption as that applied for the continuous bed. The sorbent conversions (X) and values of model parameters used for calculation were derived from the experiment.[31]

Table 4. Physical Properties and Parameters Used in Simulations

parameter	value	parameter	value
Δz	0.0005 m	α_{ads}, (weight)	0−1.0
A	2.31×10^{-3} m^2	d_p	0.06−0.179 mm
H	2.32 m	ϵ_{mf}	0.48
V_0	0.004 m^3	μ_{gas}	1.78×10^{-5} Pa s
F_{in}	0.02 mol/s	P_{M0}	0.00207 mol/(m min atm$^{0.5}$)
P	0.2−1 MPa	δ_{H_2}	25 μm
T_{set}	550 °C	E_{H_2}	9180 J/mol
S/C	4.0	P_{mem}	0.01, 0.03 MPa
ρ_{bulk}	2200 kg/m^3	$L \times Q$	206.4 mm × 50.8 mm
α_{cat}, (weight)	0−1.0	β	0−0.45

dx.doi.org/10.1021/ie500294k | Ind. Eng. Chem. Res. XXXX, XXX, XXX−XXX

Table 5. Equilibrium and Kinetic Parameters for SMR with Kinetic and Thermal Dynamic Data from Reference 47

reaction, j (in Table 3)	equilibrium constant, K_j[a]	k_{oj} (mol/(kg-cat s))	E_j (J/mol)
1	$K_1 = \exp(-26830/T + 30.114)(\text{bar}^2)$	$1.17 \times 10^{15}(\text{bar}^{0.5})$	240 100
2	$K_2 = K_1K_3$	$2.83 \times 10^{14}(\text{bar}^{0.5})$	243 900
3	$K_3 = \exp(4400/T - 4.036)(\text{bar}^2)$	$5.43 \times 10^{5}(\text{bar}^{-1})$	67 100
Van't Hoff Parameter for Species Adsorption on Catalyst			
species, i	K_{oi}[b]	ΔH_i (J/mol)	
CH_4	$6.65 \times 10^{-4}(\text{bar}^{-1})$	−38 280	
CO	$8.23 \times 10^{-5}(\text{bar}^{-1})$	−70 650	
H_2	$6.12 \times 10^{-9}(\text{bar}^{-1})$	−82 900	
H_2O	$1.77 \times 10^{5}(\text{bar}^2)$	−88 680	

[a] $k_j = k_{oj} \exp[-E_j/(RT)]$. [b] $K_i = K_{oi} \exp[-\Delta H_i/(RT)]$.

As shown in Figure 2, simulations give reasonable predictions of the CH_4 and H_2 fraction in the retentate stream. An anomalous

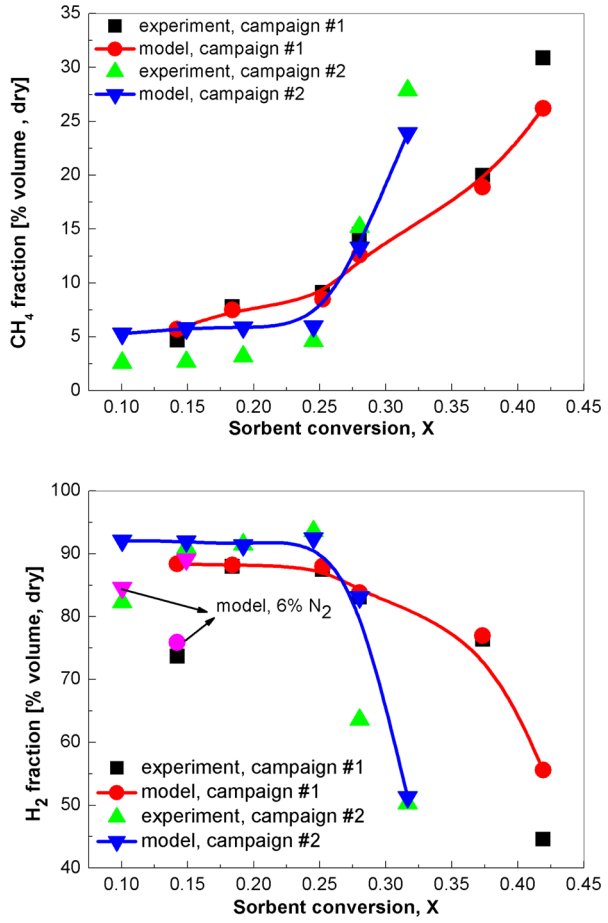

Figure 2. Comparison between experiment data and predictions.

finding in the experiment is that, for $X < 0.2$, a decreased H_2 fraction was achieved at a lower sorbent conversion, where a higher H_2 fraction was predicted by the model. When we increased the volume fraction of N_2, which was used as a pressure balance gas in the experiment, to 6% (normal value: 0.5%) in the inlet gas for calculation, the simulations agreed well with the experiment but then underpredicted the H_2 fraction for $X > 0.2$. The discrepancy for $X < 0.2$ was attributed to variation of the inlet flow rate of the natural gas or steam. Instability of the fluidization condition in bed may also lead to this variation. The trends in evolution of outlet CH_4 concentration with sorbent conversion followed the experimental results for both experimental campaigns. However, overprediction of the CH_4 conversion was observed at the breakthrough stage ($X > 0.3$). Variation of catalyst effectiveness factors during experiments may account for this overprediction.

3.2. Effect of Pressure. The following quantities are calculated to compare the performance of the reforming process under different operating conditions:

$$\text{CH}_4 \text{ conversion (\%)} = \frac{F_{\text{CH}_4,\text{in}} - F_{\text{CH}_4,\text{L}} - F_{\text{CH}_4,\text{H}}}{F_{\text{CH}_4,\text{in}}} \times 100 \tag{28}$$

$$\text{H}_2 \text{ selectivity (\%)} = \frac{F_{\text{H}_2,\text{L}} + F_{\text{H}_2,\text{H}} + F_{\text{H}_2,\text{p}}}{4F_{\text{CH}_4,\text{in}}} \times 100 \tag{29}$$

$$\text{species retentate ratio} = \frac{\text{species outlet molar flow rate}}{F_{\text{CH}_4,\text{in}}} \tag{30}$$

$$\text{sorbent utilization efficiency} = \frac{X_{\text{ex}}}{X_{\text{av}}} \tag{31}$$

$$\text{H}_2 \text{ permeation efficiency} = \frac{H_{2,\text{p}}}{H_{2,\text{p}} + F_{\text{H}_2,\text{L}} + F_{\text{H}_2,\text{H}}} \tag{32}$$

$$\text{CO}_2 \text{ capture efficiency} = \frac{\text{CO}_{2,\text{sorp}}}{\text{CO}_{2,\text{sorp}} + F_{\text{CO}_2,\text{L}} + F_{\text{CO}_2,\text{H}}} \tag{33}$$

Note that the species in eq 30 include CH_4, H_2O, H_2, CO_2, and CO. In eq 32, the H_2 permeation efficiency is defined as the H_2 flux in the permeate line divided by the sum of the H_2 flux in permeate line and in the outlet stream of the reformer. Lastly, note that, in eq 33, the CO_2 capture efficiency is defined as the carbon difference between the inlet and outlet of the reformer divided by the sum of CO_2 adsorbed by sorbent and retentate CO_2 in the outlet stream of the reformer.

The maximum practical operating tempeture for the membrane is ~650 °C, while a temperature of >500 °C is required to obtain efficient CO_2 capture by CaO. Taking the design conditions of the reformer into consideration, the operating temperature window for a sorption-enhanced FBMR is ~500−600 °C. In this work, the temperature was set at 550 °C, which is much lower than that for a standard industrial SMR.[31] The temperature distribution in a fluidized-bed reactor is much more uniform than for a fixed-bed reactor, so a constant temperature is assumed in the following simulations. A steam-to-carbon (S/C) ratio of ~3 is commonly used in steam reforming of natural gas[21] at temperatures of >650 °C. To reduce the production of CO, we adopted a higher S/C ratio of 4. A carbon balance for the system investigated showed that the CO_2 reacted in the bed and carbon removed from the gas matched in the noted cases.

Figure 3 presents CH_4 conversion profiles along the reactor for four different reforming processes (SMR, SE-SMR, MA-SMR, and MA-SE-SMR). The distribution of membrane panels along the reactor is not continuous, leading to nonsmooth CH_4

dx.doi.org/10.1021/ie500294k | Ind. Eng. Chem. Res. XXXX, XXX, XXX−XXX

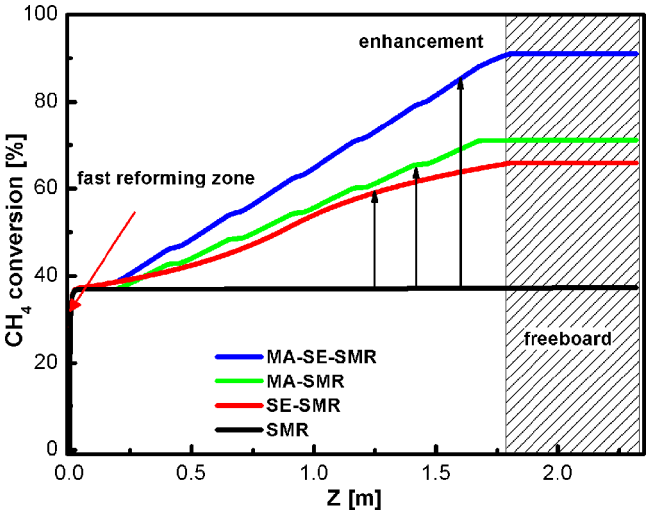

Figure 3. Predicted CH_4 conversion at different heights above the distributor ($P = 0.6$ MPa, $\alpha_{ads} = 0.5$, $\beta = 0.28$, $m_s = 3.87$ kg/h, $m_0 = 0.0194$ kg/h, $Feed_{CH_4,in} = 0.034$ Nm^3/h).

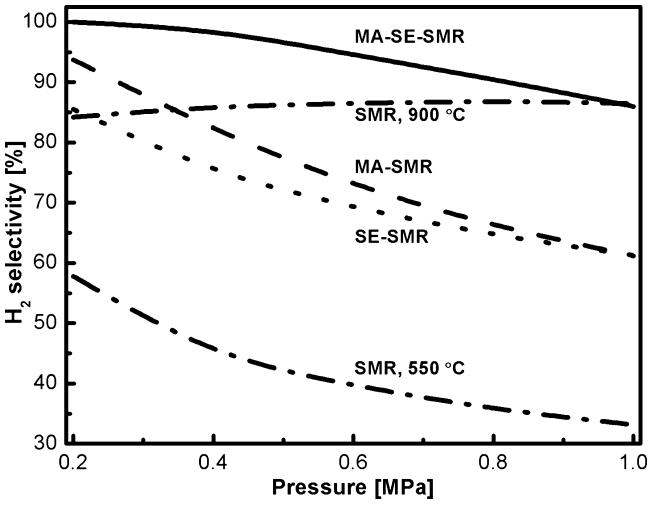

Figure 4. Predicted effect of inlet pressure on H_2 selectivity of four operating conditions ($\alpha_{ads} = 0.5$, $\beta = 0.28$, $m_s = 3.87$ kg/h, $m_0 = 0.0194$ kg/h, $Feed_{CH_4,in} = 0.034$ Nm^3/h).

conversion curves. Based on correlation (9), as well as correlations (14) and (15), the ratios of sorbent recycle rate and fresh sorbent feed rate to the methane feed rate, on a molar basis, are 4 and 0.04, respectively. Enhancing effects of H_2 separation and CO_2 removal on the reforming process are clearly indicated by the continued conversion of CH_4 after a rapid steam reforming stage. A CH_4 conversion of 91.4% is achieved for 0.6 MPa and 550 °C, with both the sorbent and membrane acting simultaneously, while only 37.1% conversion is observed for SMR with neither enhancement. The conversion of CH_4 in the freeboard changes somewhat from the value at the bed surface. This can be explained by

(1) After the fast reforming zone, the SMR reactions are dominated by thermodynamic equilibrium. We assume only minor temperature variation in a fluidized bed.
(2) Compared with the reforming reactions, CO_2 capture kinetics are too slow, at such a low concentration (0.1%, by volume) in the freeboard region, to break the equilibrium.
(3) No membrane panels are installed in the freeboard region, so no effect of membrane assistance is observed.

In the MA-SE-SMR, H_2 separation and CO_2 capture are integrated and coupled with steam reforming in a fluidized-bed reactor. Both enhancement techniques affect each other, augmenting the reforming efficiency. High pressure is helpful to improve the throughput for industrial production. However, pressure also has a profound influence on the behavior of the reactions. Higher pressure suppresses the conversion of CH_4 in the SMR, but favors H_2 permeation and CO_2 sorption. For MA-SE-SMR, the influence of pressure results from a combination of all three effects. Figure 4 indicates that, when H_2 separation and CO_2 capture are combined with reforming, nearly 100% H_2 selectivity is possible for pressures of <0.4 MPa, which is an improvement over SMR at the standard operation temperature of ~900 °C. At the same time, the CO_2 emissions from MA-SE-SMR are much lower than for either MA-SMR or SMR, but are slightly higher than that observed for SE-SMR at pressures of <0.4 MPa, as shown in Figure 5a. The main reason is that membrane separation is able to enhance the SMR process to a greater extent than with sorbent alone, resulting in quicker CO_2 production, exceeding the capture capacity of sorbent for the specified temperature and pressure. Hence, to approach zero-carbon emission in a single unit, the effect of H_2 permeation must be taken into account when specifying the sorbent loading.

Simulations indicate that the suppression effect of pressure on the reforming equilibrium overwhelms the enhancing effect of CO_2-sorption and H_2-membrane separation as the pressure continues to increase, resulting in decreased H_2 selectivity for pressures of >0.4 MPa. As illustrated in Figure 5, the retentate CO_2 ratios are close to zero for SE-SMR, but full conversion of CH_4 is still hard to achieve. This indicates that the enhancing effect of sorption on CH_4 conversion is limited at high pressure. This is not restricted by the capture kinetics, which are sufficiently fast for the cases studied. Comparing the CO retentate ratios in Figure 5b, CO_2 sorption shows greater ability to reduce CO production than membrane separation with an effectiveness factor of 0.28.

To gain further insight into the influence of pressure on membrane separation and CO_2 capture, the H_2 permeation efficiency and CO_2 capture efficiency for four different processes are compared in Figure 6. The permeation rate of H_2 increases with pressure to the power of 0.5,[20] whereas CO_2 capture depends on the pressure in a first-order manner.[4] Gas molar concentration also increases with pressure almost linearly. As a result, for the MA-SMR, despite the H_2 permeation flux increasing with increasing H_2 partial pressure, the $H_{2,p}/H_{2,total}$ ratio decreases due to the limited effective membrane permeation area of membrane, as shown in Figure 6. Therefore, the H_2 retentate ratio does not decrease dramatically, although the conversion of CH_4 was suppressed by the higher pressure. For MA-SE-SMR, because more H_2 is generated as a result of adding the sorbent, the H_2 retentate ratio is predicted to increase as the pressure increases. The permeation efficiency of MA-SE-SMR decreases with increasing pressure more quickly than for MA-SMR, indicating that greater effective permeation area is required. The CO_2 capture efficiency increases with the increasing pressure, until almost 100% efficiency is achieved. Increasing the effective permeation area of the membrane is the key to effective operation at higher pressures. Since the CO_2 capture kinetics are sufficiently fast at the specified temperature, increasing the effective permeation area of the membrane is

dx.doi.org/10.1021/ie500294k | Ind. Eng. Chem. Res. XXXX, XXX, XXX−XXX

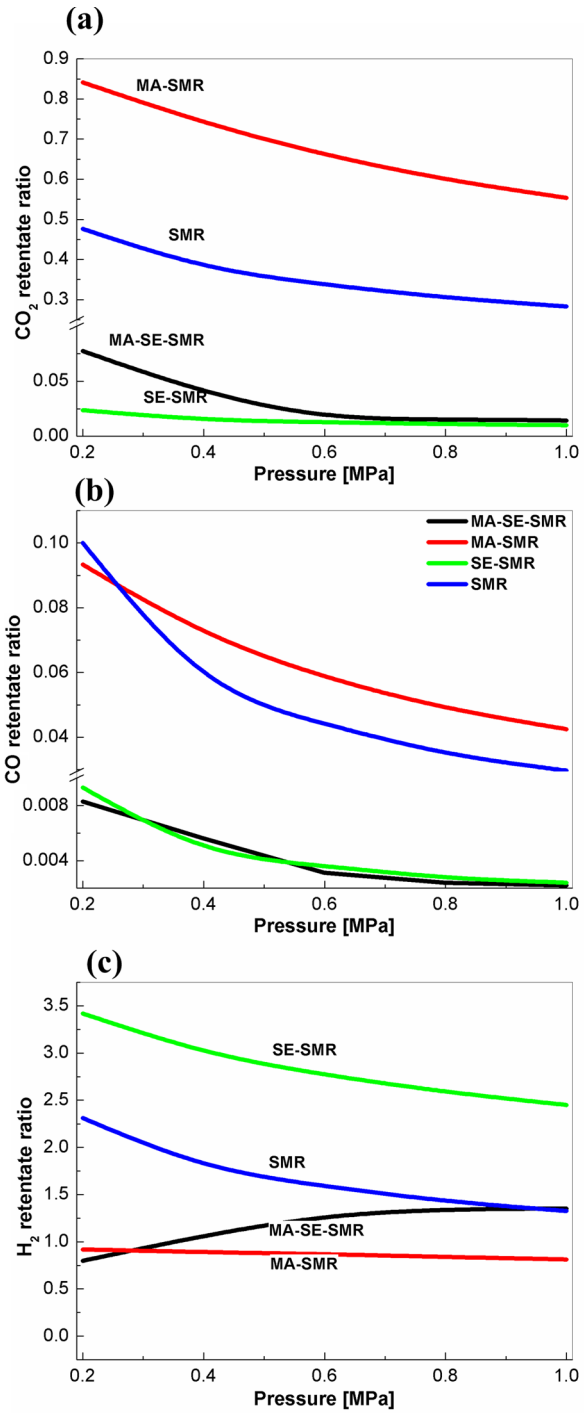

Figure 5. Predicted influence of inlet pressure on (a) CO_2 retentate ratio, (b) CO retentate ratio, and (c) H_2 retentate ratio of MA-SE-SMR ($\alpha_{ads} = 0.5$, $\beta = 0.28$, $m_s = 3.87$ kg/h, $m_0 = 0.0194$ kg/h, $Feed_{CH_4,in} = 0.034$ Nm^3/h).

extremely important for improving the H_2 productivity of MA-SE-SMR at higher pressures.

3.3. Effect of Sorbent Fraction, Effective Area of Membrane, and Gas Feed Rate. Figures 6 and 7 show the predicted effect of sorbent loading on the performance of the MA-SE-SMR process in a continuous fluidized bed with different membrane effectiveness factors. While the sorbent mass fraction varied, the initial bed volume was maintained constant (i.e., the relative proportions of catalyst and sorbent were varied). With

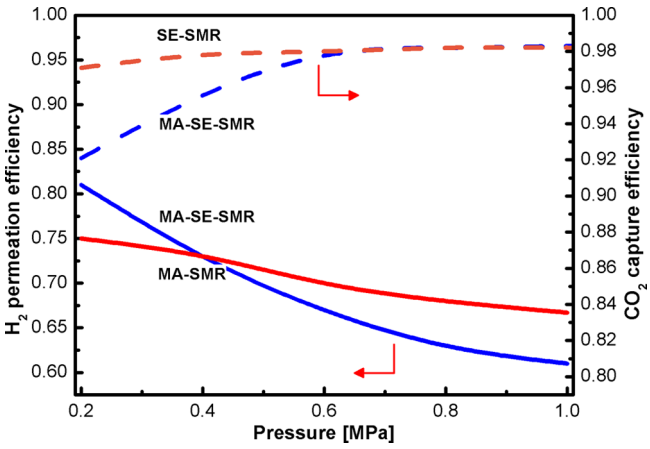

Figure 6. Predicted influence of inlet pressure on permeation efficiency and capture efficiency ($\alpha_{ads} = 0.5$, $\beta = 0.28$, $m_s = 3.87$ kg/h, $m_0 = 0.0194$ kg/h, $Feed_{CH_4,in} = 0.034$ Nm^3/h).

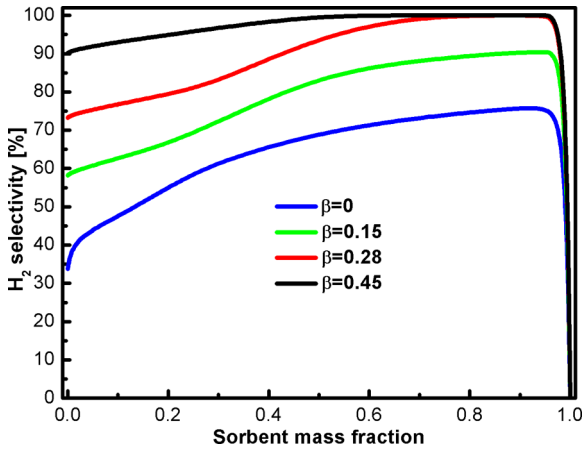

Figure 7. Predicted effect of sorbent mass fraction on H_2 selectivity for MA-SE-SMR with different membrane effectiveness factors ($P = 0.6$ MPa, $m_s = 3.87$ kg/h, $m_0 = 0.0194$ kg/h, $Feed_{CH_4,in} = 0.034$ Nm^3/h).

more sorbent present, the H_2 productivity improved, as shown in Figure 7, which is consistent with earlier work.[4,15,54] The maximum conversion for a given sorbent is determined by the sorbent recycling rate and the fresh sorbent feed rate. The fraction of active sorbent (f_a) is also determined by the total sorbent in the bed and the sorbent recycle rate. Note that the upper limit of effective conversion of sorbent is strictly constrained by the sorbent feed rate ($F_R + F_0$) for steady-state operation. Since the solids cycle between the reformer and regenerator without separation of catalyst, increasing the sorbent fraction means increasing the sorbent recycle rate. However, a dramatic drop of H_2 selectivity occurred when the sorbent fraction exceeded 0.95, because of a more dilute distribution of catalyst in the bed. Proper CO_2 capture capacity, which depends on the in-bed sorbent weight fraction for given sorbent and temperature, is necessary to reduce the CO_2 and CO production, as seen in Figure 8. A sorbent mass fraction of >0.7 is required for $\beta = 0.28$ to achieve a H_2 selectivity of >98% with very low CO_2 + CO emissions.

The influence of gas feed rate on the reforming process is presented in Figure 9. The superficial velocity is ~0.25 m/s when the total gas feed rate increases to 0.516 Nm^3/h. Bubbling fluidization is still expected.[37] Increasing the inlet flow rate results in bigger bubbles, causing more bypass. When the sorbent

dx.doi.org/10.1021/ie500294k | Ind. Eng. Chem. Res. XXXX, XXX, XXX−XXX

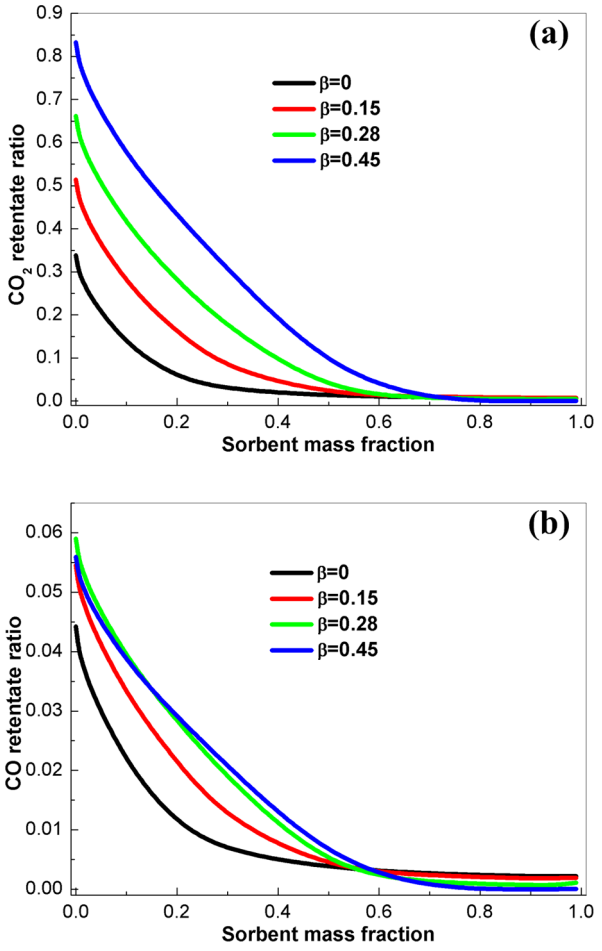

Figure 8. Predicted effect of sorbent fraction on (a) CO_2 retentate ratio and (b) CO retentate ratio of MA-SE-SMR with different membrane effectiveness factors (P = 0.6 MPa, m_s = 3.87 kg/h, m_0 = 0.0194 kg/h, $Feed_{CH_4,in}$ = 0.034 Nm^3/h).

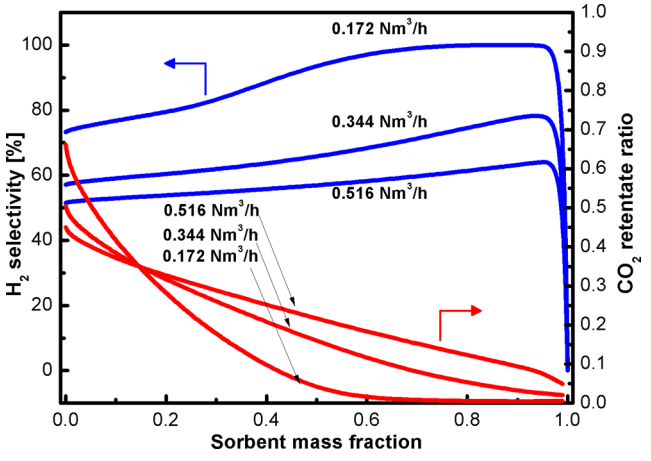

Figure 9. Predicted effect of sorbent fraction on MA-SE-SMR performance with different gas feed rates (P = 0.6 MPa, β = 0.28, m_s = 3.87 kg/h, m_0 = 0.0194 kg/h).

concentration is low, less CO_2 is produced at higher total gas feed rate due to the limited SMR reaction. More CO_2 leaves the reactor at higher total gas feed rate when the sorbent concentration is high, bceause of the relatively slow reaction kinetics of carbonation, compared with SMR.

3.4. Effects of Sorbent Recycling Rate, Fresh Sorbent Feed Rate, and In-Bed Sorbent Loading. Detailed investigation is required to systematically study the effect of CO_2 capture on reforming, especially when the influences of fresh sorbent feed rate and sorbent in-bed loading are taken into account. Figures 10 and 11 shows the effects of sorbent recycle

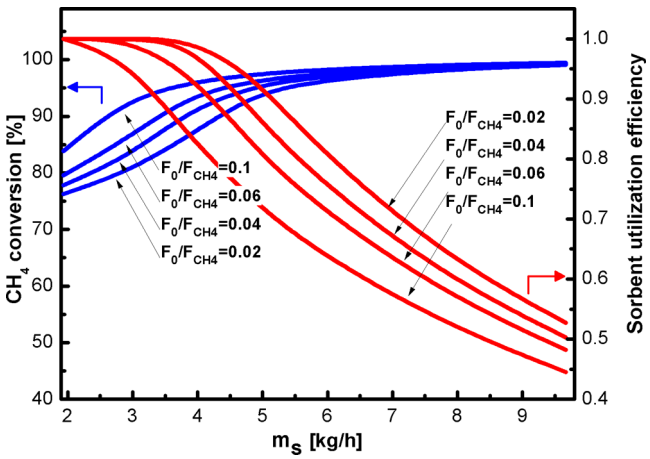

Figure 10. Predicted effect of sorbent recycling rate on the MA-SE-SMR performance with different fresh sorbent feed rates (P = 0.6 MPa, α_{ads} = 0.5, β = 0.28, $F_{CH_4,in}$ = 0.034 Nm^3/h).

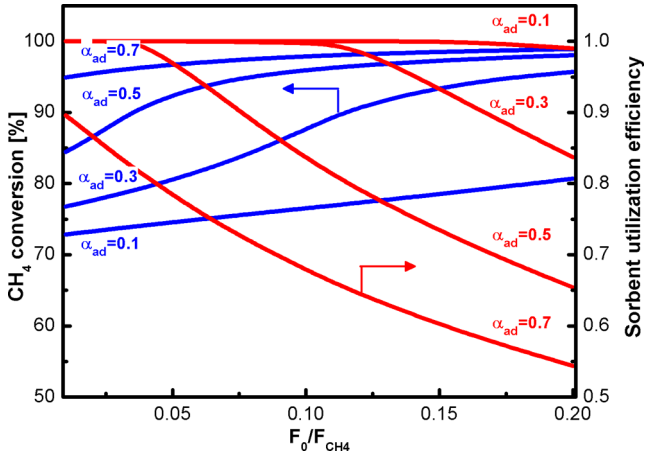

Figure 11. Predicted effect of fresh sorbent feed rate on MA-SE-SMR performance with different sorbent fractions (P = 0.6 MPa, β = 0.28, m_s = 3.87 kg/h, m_0 = 0.0194 kg/h, $Feed_{CH_4,in}$ = 0.034 Nm^3/h).

rate and fresh sorbent feed rate on CH_4 conversion and sorbent utilization efficiency. To account for the effect of sorbent fraction, the solids recycle flux (m_s) is fixed at 3.87 kg/h in Figure11.

Increasing the recycle flux of sorbent, leading to more active sorbent in the reformer, is an efficient way to improve the CH_4 conversion, as indicated in Figure 10. However, more underutilized sorbent appears in the outlet stream for higher recycle rates. Higher H_2 selectivity is desirable, but optimizing the sorbent utilization efficiency is essential to reduce cost.[55] Another problem with a higher sorbent recycling rate is that more heat is required to heat the sorbent transferred from the reformer to the calcination temperature. Adding more fresh sorbent in the solid flux entering the reformer is helpful to augment the CH_4 conversion for moderate sorbent recycling rates, but it also increases the cost. Another practicable way is to

dx.doi.org/10.1021/ie500294k | Ind. Eng. Chem. Res. XXXX, XXX, XXX−XXX

increase the sorbent fraction in the solids, as indicated in Figure 11, but not so far that the catalyst amount become rate-limiting. The synergistic influence of $F_R/F_{CH_4,in}$ and $F_0/F_{CH_4,in}$. on the efficiency of the entire system need to be taken into account when determining the operating parameters.

3.5. Effect of Permeation Pressure. From eq 2, the H_2 permeation rate is profoundly affected by $P_{H_2,p}$, the H_2 partial pressure on the permeate side. Figures 12 and 13 show the predicted influence of $P_{H_2,p}$ on the in-bed CH_4 conversion and the production of CO_2 and CO. Decreasing $P_{H_2,p}$ favors H_2 permeation, promoting CH_4 conversion and the water-gas-shift reaction. However, more energy is required to attain a lower $P_{H_2,p}$, as well as for subsequent product compression. According to Sieverts' Law,[20] decreasing the thickness of the membrane layer would improve the permeation rate. However, a thinner membrane is likely to have lower selectivity and be more prone to be damaged, especially in a fluidized bed where the fluidized particles exert external stress on the surface of the membrane. Therefore, one must be careful to apply extra thin membranes in a fluidized-bed reactor.

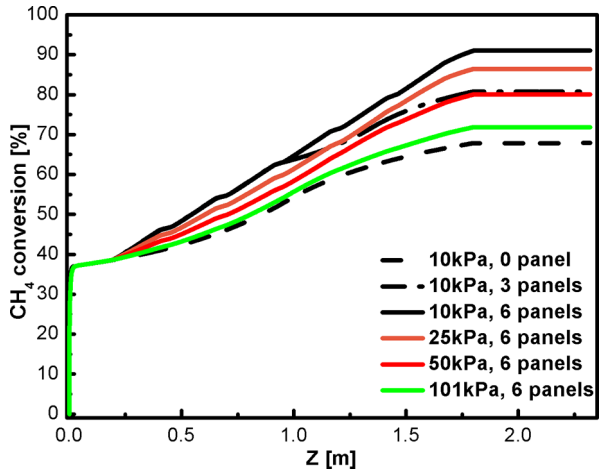

Figure 12. Predicted effect of permeation pressure and number of membranes on CH_4 conversion of MA-SE-SMR (P = 0.6 MPa, α_{ads} = 0.5, β = 0.28, m_s = 3.87 kg/h, m_0 = 0.0194 kg/h, $Feed_{CH_4,in}$ = 0.034 Nm^3/h).

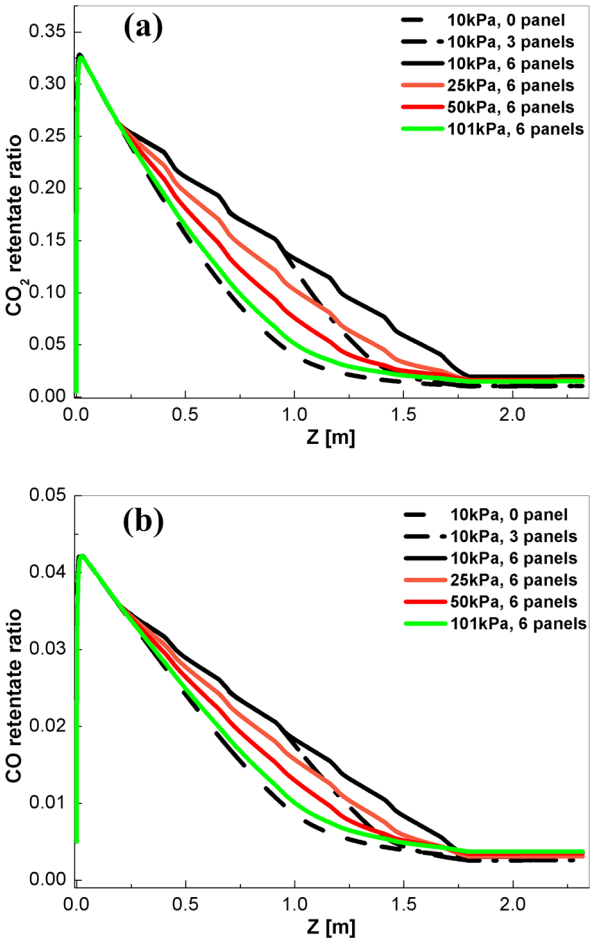

Figure 13. Predicted effect of permeation pressure and number of membranes on the (a) CO_2 retentate ratio and (b) CO retentate ratio of MA-SE-SMR (P = 0.6 MPa, α_{ads} = 0.5, β = 0.28, m_s = 3.87 kg/h, m_0 = 0.0194 kg/h, $Feed_{CH_4,in}$ = 0.034 Nm^3/h).

3.6. Sensitivity Analysis. The sensitivities of CH_4, CO_2, and CO profiles were investigated, with respect to variations in particle diameter (d_p), sorption kinetic rate constant (k_0), and membrane effectiveness factor (β).

Sensitivity analysis can identify conditions that can most improve the MA-SE-SMR performance. A pre-exponential rate constant of k_0 = 3.5 was used in previous cases. Decreasing k_0 leads to more CO, CO_2, and CH_4 in the off-gas product, because of decreased CO_2 capture. However, the CH_4 conversion with k_0 = 3.5 × 10^{-2} was almost the same as that observed for k_0 = 3.5. The main reason is that the CO_2 capture rate depends greatly on the sorbent feed rate ($F_R + F_0$), illustrated in Figure 14a, the CH_4 conversion is very sensitive to the effective membrane area. More CO was produced from membrane-enhanced SMR, but the additional CO was converted to CO_2 via the water-gas-shift reaction, enhanced by H_2 separation, as indicated in Figure 14c. For a membrane effectiveness factor of <0.28, fast sorption kinetics are extremely important to reduce the CO emissions. . Within the bubbling fluidization regime, particle size affects the reforming process only slightly for the limited range investigated. In practice, limestone is prone to serious attrition under continuous operation. The resulting reduction in particle size affects the flow structure greatly, possibly even changing the flow regime; hence, it is important to constrain sorbent attrition, e.g., by additives or pelletization. In addition, the change of particles density during MA-SE-SMR due to CO_2 sorption and coke deposition may also change the fluidization conditions.

Several issues should be taken seriously to make MA-SE-SMR practical, although they are simplified when performing simulations. In addition to the desirability of improving permeation efficiency, innovations in synthesizing method and materials would help to improve the lifetime of membranes exposed to particles. When two types of particles (catalyst and sorbent) coexist in the system, segregation is readily to occur, which could reduce the reaction efficiency significantly. Sorbent attrition and catalyst deactivation could also seriously hamper the process if not limited.

4. CONCLUSIONS

A simplified generic kinetic model is imposed to simulate continuous membrane-assisted sorbent-enhanced steam methane reforming (MA-SE-SMR) in a catalytic fluidized-bed reformer. Simulation results show reasonable agreement with the limited available experimental results.

dx.doi.org/10.1021/ie500294k | Ind. Eng. Chem. Res. XXXX, XXX, XXX−XXX

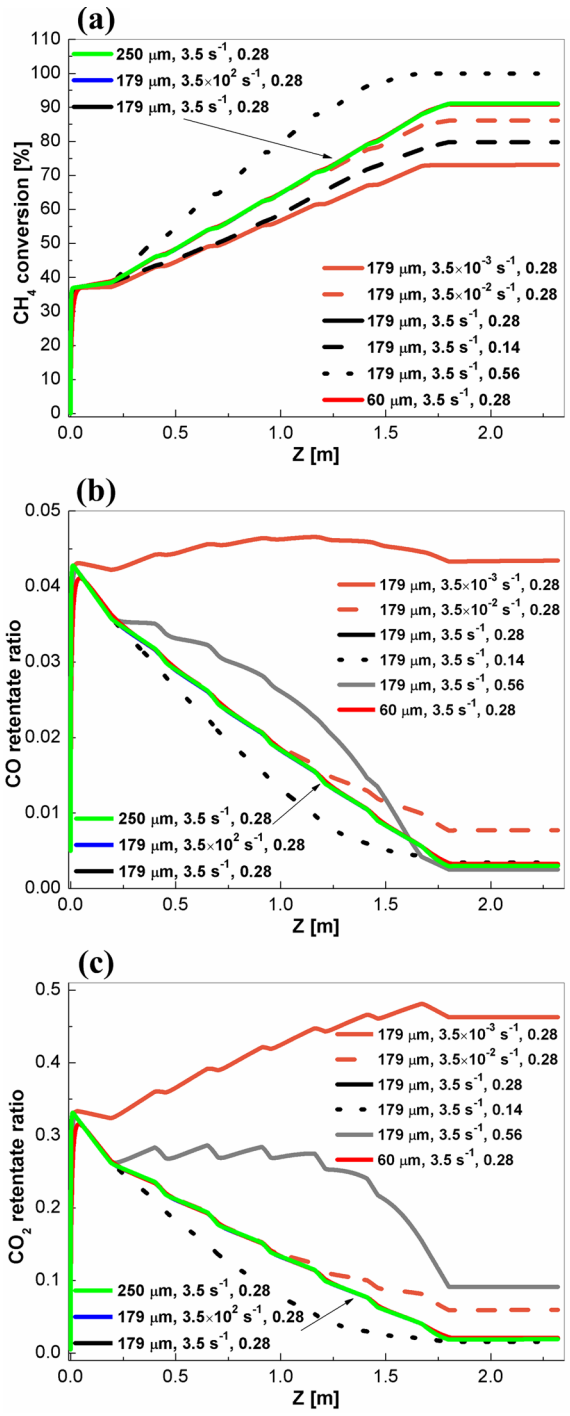

Figure 14. Sensitivity analysis results for CH_4 conversion, CO_2 production, and CO production for variations in particle diameter, sorption rate constant, and membrane effectiveness factor (P = 0.6 MPa, α_{ads} = 0.5, m_s = 3.87 kg/h, m_0 = 0.0194 kg/h, $Feed_{CH_4,in}$ = 0.034 Nm^3/h).

It is shown that a product stream with >98% H_2 selectivity containing almost no CO_2 and CO can be obtained for operating conditions of T = 550 °C, P = 0.6 MPa with CO_2 capture and H_2 permeation integrated with steam reforming. CaO exhibits promising CO_2 capture efficiency at this temperature for all pressures considered (0.2−1.0 MPa). Membrane separation shows potential to maintain high H_2 productivity at high operating pressures. However, the separation efficiency—and, hence, H_2 generation—are limited by the membrane effectiveness factor. A high sorbent recycling rate is desirable to improve CH_4 conversion, but must be optimized to limit the energy cost, while maintaining the sorbent utilization efficiency. Adding more fresh sorbent is helpful to increase the H_2 productivity, but adds to the cost. For a fixed recycle rate of solids (catalyst, sorbent, and inerts), increasing the sorbent fraction of the solids can improve the conversion of CH_4, but enough catalyst must be provided that it does not become rate-limiting. Increasing the partial pressure of hydrogen in the permeate stream leads to a decrease in CH_4 conversion, because of decreased H_2 permeation.

Sensitivity analysis demonstrated that, for the operating conditions studied, the MA-SE-SMR performance is more sensitive to the membrane effectiveness factors than to the kinetics of sorbent. The CO_2 capture rate is affected greatly by the total sorbent feed rate. Quick sorption kinetics helps to reduce CO production.

AUTHOR INFORMATION

Corresponding Author

*Tel.: 86-27-87542417. Fax: 86-27-87545526. E-mail: jyzhang@hust.edu.cn.

Notes

The authors declare no competing financial interest.

ACKNOWLEDGMENTS

This work was supported by the National Key Basic Research Program (2010CB227003) and National Science Foundation of China (41172140, 50906031). We thank the China Scholarship Council (CSC) for financial support to Yumin Chen for visiting study at the University of British Columbia.

NOMENCLATURE

Latin Symbols

A = cross-sectional area, m^2
A_p = permeation area per unit length, m^2
A_b = area of bubble, m^2
C_i = concentration of species i, mol/m^3
d_p = particle diameter, m
d_b = bubble diameter, m
d_{bm} = maximum bubble diameter, m
D_{ij} = binary diffusion coefficient, m^2/s
D_e = effective diffusivity, m^2/s
E_{H_2} = activation energy for hydrogen permeation, J/mol
E_j = activation energy for chemical reaction j, J/mol
F_i = molar flow rate of species i, mol/s
F_{in} = inlet molar flow rate, mol/s
m_s = recycle mass rate of solids, kg/h
F_R = recycle molar rate of sorbent, mol/s
m_0 = feed mass rate of fresh sorbent, kg/h
F_0 = feed molar rate of fresh sorbent, mol/s
$F_{CH4,in}$ = inlet mole flow rate of methane, mol/s
$Feed_{CH4,in}$ = inlet volumetric flow rate of methane, Nm^3/h
F_{in} = total gas feed rate, Nm^3/h
f_a = fraction of active sorbent in bed
H = total column height, m
ΔH_i = heat of reaction for reaction i, J/mol
J = H_2 permeation flux, $mol/(m^2\ s)$
k_{iq} = interphase mass transfer coefficient for species i, m/s
k_w = wake-emulsion exchange coefficient, 1/s
k_j = pre-exponential factor for rate constant of chemical reaction j, 1/s
k_{cap} = rate constant for gas−solid surface reaction, m/s

dx.doi.org/10.1021/ie500294k | Ind. Eng. Chem. Res. XXXX, XXX, XXX−XXX

L_0 = length of the reformer, m
N_ϕ = number of chemical species considered in modeling
P = overall pressure, Pa
P_{M0} = pre-exponential factor for permeation, mol/(m min atm$^{0.5}$)
P_{mem} = pressure on permeate side of membrane, Pa
Q_{req} = minimum volumetric flow rate r maintaining fluidization, m^3/s
$Q_{H,L}$ = volumetric flow rate of phases H and L, m^3/s
r_N = mass fraction of particles (circulated for N times) in the inlet sorbent stream
T_{set} = average bed temperature, °C
U_b = bubble velocity, m/s
U_{mf} = minimum fluidization velocity, m/s
V_0 = initial bed loading of solid, m^3
X = conversion of CaO
X_N = ultimate conversion of CaO after N cycles
X_{ex} = conversion of CaO in outlet stream of sorbents
$X_{in,i}$ = species mole fraction in inlet of reformer, i = CH_4, H_2O, CO_2, CO, H_2, N_2

Greek Symbols

α_{cat} = weight fraction of catalyst in solids
α_{ads} = weight fraction of sorbent in solids
β = membrane effectiveness factor
ρ_s = bulk density of solid particles, kg/m^3
$\rho_{m,CaO}$ = molar density of sorbent, mol CaO/m^3
ε_{mf} = bed voidage at minimum fluidization velocity
$\varepsilon_{H,L}$ = voidage of phases H and L
ε_T = total voidage of bed; $\varepsilon_T = \psi_H\varepsilon_H + \psi_L\varepsilon_L$
$\psi_{H,L}$ = volume fraction of bed occupied by phases H and L
μ_{gas} = gas viscosity, Pa s
δ_{H_2} = thickness of membranes, m

Abbreviations

FBMR = fluidized bed membrane reactor
cat = catalyst
SMR = steam methane reforming
SE = sorption enhanced
MA = membrane assisted
RTD = residence time distribution
vol = volume

REFERENCES

(1) Holladay, J. D.; Hu, J.; King, D. L.; Wang, Y. An overview of hydrogen production technologies. *Catal. Today* **2009**, *139*, 244−260.
(2) Scura, F.; Barbieri, G.; Drioli, E. H_2 for PEM-FC: Effect of CO in the purification by means of Pd-based membranes. *Desalination* **2006**, *200*, 239−241.
(3) National Research Council. *The Hydrogen Economy: Opportunities, Costs, Barriers, and R&D Needs*; National Acadamies Press: Washington, DC, 2004.
(4) Johnsen, K. Sorption-enhanced steam methane reforming in fluidized bed reactor. Ph.D. Thesis, Norwegian University of Science and Technology, Trondheim, Norway, 2006.
(5) Harrison, D. P. Sorption-enhanced hydrogen production: A review. *Ind. Eng. Chem. Res.* **2008**, *47*, 6486−6501.
(6) Thomsen, V. B. E. LeChâtelier's principle in the sciences. *J. Chem. Educ.* **2000**, *77*, 173−176.
(7) Balasubramanian, B.; Ortiz-Lopez, A.; Kaytakoglu, S.; Harrison, D. P. Hydrogen from methane in a single-step process. *Chem. Eng. Sci.* **1999**, *54*, 3543−3552.
(8) Martavaltzi, C. S.; Pampaka, E. P.; Korkakaki, E. S.; Lemonidou, A. A. Hydrogen production via steam reforming of methane with simultaneous CO_2 capture over CaO−$Ca_{12}Al_{14}O_{33}$. *Energy Fuels* **2010**, *24*, 2589−2595.
(9) Essaki, K.; Muramatsu, T.; Kato, M. Effect of equilibrium shift by using lithium silicate pellets in steam methane reforming. *Int. J. Hydrogen Energy* **2008**, *33*, 4555−4559.
(10) Ding, Y.; Alpay, E. Adsorption-enhanced steam methane reforming. *Chem. Eng. Sci.* **2000**, *55*, 3929−3940.
(11) Arstad, B.; Prostak, J.; Blom, R. Continuous hydrogen production by sorption enhanced steam methane reforming (SE-SMR) in a circulating fluidized bed reactor: Sorbent to catalyst ratio dependencies. *Chem. Eng. J.* **2012**, *189*−*190*, 413−421.
(12) Lee, D. K.; Baek, I. H.; Yoon, W. L. Modeling and simulation for the steam methane reforming enhanced by in situ CO_2 removal utilizing the CaO carbonation for H_2 production. *Chem. Eng. Sci.* **2004**, *59*, 931−942.
(13) Ochoa-Fernández, E.; Rusten, H. K.; Jakobsen, H. A.; Rønning, M.; Holmen, A.; Chen, D. Sorption enhanced hydrogen production by steam methane reforming using Li_2ZrO_3 as sorbent: sorption kinetics and reactor simulation. *Catal. Today* **2005**, *106*, 41−46.
(14) Johnsen, K.; Ryu, H. J.; Grace, J. R.; Lim, C. J. Sorption-enhanced steam reforming of methane in a fluidized bed reactor with dolomite as CO_2-acceptor. *Chem. Eng. Sci.* **2006**, *61*, 1195−1202.
(15) Carlo, A. D.; Bocci, E.; Zuccari, F.; Dell'Era, A. Numerical investigation of sorption enhanced steam methane reforming process using computational fluid dynamics Eulerian−Eulerian code. *Ind. Eng. Chem. Res.* **2010**, *49*, 1561−1576.
(16) Wang, Y. F.; Chao, Z. X.; Jakobsen, H. A. 3D Simulation of bubbling fluidized bed reactors for sorption enhanced steam methane reforming processes. *J. Nat. Gas Sci. Eng.* **2010**, *2*, 105−113.
(17) Wang, Y. F.; Chao, Z. X.; Chen, D.; Jakobsen, H. A. SE-SMR process performance in CFB reactors: Simulation of the CO_2 adsorption/desorption processes with CaO based sorbents. *Int. J. Greenhouse Gas Control* **2011**, *5*, 489−497.
(18) Adris, A. M.; Lim, C. J.; Grace, J. R. The fluidized bed membrane reactor system: A pilot scale experimental study. *Chem. Eng. Sci.* **1994**, *49*, 5833−5843.
(19) Roses, L.; Gallucci, F.; Manzolini, G.; van Sint Annaland, M. Experimental study of steam methane reforming in a Pd-based fluidized bed membrane reactor. *Chem. Eng. J* **2013**, *222*, 307−320.
(20) Sieverts, A.; Zapf, G. The solubility of deuterium and hydrogen in solid palladium. *Z. Phys. Chem.* **1935**, *174*, 359−364.
(21) Rakib, M. A.; Grace, J. R.; Lim, C. J.; Elnashaie, S. S. E. H. Steam reforming of heptane in a fluidized bed membrane reactor. *J. Power Sources* **2010**, *195*, 5749−5760.
(22) Rakib, M. A.; Grace, J. R.; Lim, C. J.; Elnashaie, S. S. E. H.; Ghiasi, B. Steam reforming of propane in a fluidized bed membrane reactor for hydrogen production. *Int. J. Hydrogen Energy* **2010**, *35*, 6276−6290.
(23) Mahecha-Botero, A.; Boyd, T.; Gulamhusein, A.; Comyn, N.; Lim, C. J.; Grace, J. R.; Shirasaki, Y.; Yasuda, I. Pure hydrogen generation in a fluidized-bed membrane reactor: Experimental findings. *Chem. Eng. Sci.* **2008**, *63*, 2752−2762.
(24) Mahecha-Botero, A.; Boyd, T.; Gulamhusein, A.; Grace, J. R.; Lim, C. J.; Shirasaki, Y.; Kurokawa, H.; Yasuda, I. Catalytic reforming of natural gas for hydrogen production in a pilot fluidized-bed membrane reactor: Mapping of operating and feed conditions. *Int. J. Hydrogen Energy* **2011**, *36*, 10727−10736.
(25) Grace, J. R.; Li, X. T.; Lim, C. J. Equilibrium modeling of catalytic steam reforming of methane in membrane reactors with oxygen addition. *Catal. Today* **2001**, *64*, 141−149.
(26) Chen, Z.; Yan, Y.; Elnashaie, S. S. E. H. Modeling and optimization of a novel membrane reformer for higher hydrocarbons. *AIChE J.* **2003**, *49*, 1250−1265.
(27) Adris, A. M.; Lim, C. J.; Grace, J. R. The fluidized-bed membrane reactor for steam methane reforming: Model verification and parametric study. *Chem. Eng. Sci.* **1997**, *52*, 1609−1622.
(28) Rakib, M. A.; Grace, J. R.; Lim, C. J.; Elnashaie, S. S. E. H. Modeling of a fluidized bed membrane reactor for hydrogen production by steam reforming of hydrocarbons. *Ind. Eng. Chem. Res.* **2011**, *50*, 3110−3129.
(29) Mahecha-Botero, A.; Chen, Z. X.; Grace, J. R.; Elnashaie, S. S. E. H.; Lim, C. J.; Rakib, M. B.; Yasuda, I.; Shirasaki, Y. Comparison of

fluidized bed flow regimes for steam methane reforming in membrane reactors: A simulation study. *Chem. Eng. Sci.* **2009**, *64*, 3508−3613.
(30) Mahecha-Botero, A.; Grace, J. R.; Lim, C. J.; Elnashaie, S. S. H. E.; Boyd, T.; Gulamhusein, A. Pure hydrogen generation in a fluidized bed reactor: Application of the generalized comprehensive reactor model. *Chem. Eng. Sci.* **2009**, *64*, 3826−3846.
(31) Mahecha-Botero, A.; Boyd, T.; Grace, J. R.; Lim, C. J.; Gulamhusein, A.; Wan, B.; Kurokawa, H.; Shirasaki, Y. In-situ CO_2 capture in a pilot-scale fluidized-bed membrane reformer for ultra-pure hydrogen production. *Int. J. Hydrogen Energy* **2011**, *36*, 4038−4055.
(32) Toomey, R. D.; Johnstone, H. F. Gaseous fluidization of solid particles. *Chem. Eng. Prog.* **1952**, *48*, 220−226.
(33) Grace, J. R. Generalized models for isothermal fluidized bed reactors. In *Recent Advances in the Engineering Analysis of Chemically Reacting Systems*; Doraiswamy, L. K., Ed.; Wiley: New Delhi, India, 1984; pp 237−255.
(34) Pugsley, T. S.; Patience, G. S.; Berruti, F.; Chaouki, J. Modeling the catalytic oxidation of n-butane to maleic anhydride in a circulating fluidized bed reactor. *Ind. Eng. Chem. Res.* **1992**, *31*, 2652−2660.
(35) Abba, I. A.; Grace, J. R.; Bi, H. T. Variable-gas-density fluidized bed reactor model for catalytic processes. *Chem. Eng. Sci.* **2002**, *57*, 4797−4807.
(36) Adris, A. M.; Lim, C. J.; Grace, J. R. The fluidized-bed membrane reactor for steam methane reforming: Model verification and parametric study. *Chem. Eng. Sci.* **1997**, *52*, 1609−1622.
(37) Abba, I. A.; Grace, J. R.; Bi, H. T. Spanning the flow regimes: Generic fluidized-bed reactor model. *AIChE J.* **2003**, *49*, 1838−1848.
(38) Abba, I. A.; Grace, J. R.; Bi, H. T. Application of the generic fluidized-bed reactor model to the fluidized-bed membrane reactor process for steam methane reforming with oxygen input. *Ind. Eng. Chem. Res.* **2003**, *42*, 2736−2745.
(39) Wen, C. Y.; Yu, Y. H. A. A generalized method for predicting minimum fluidization velocity. *AIChE J.* **1966**, *3*, 610−612.
(40) Grace, J. R. Fluidized-Bed Hydrodynamics. In *Handbook of Multiphase Systems*; Hetsroni, G., Ed.; Hemisphere Publishing: Washington, DC, 1982; Chapter 8.1, pp 5−64.
(41) Sit, S. P.; Grace, J. R. Effect of bubble interaction on interphase mass transfer in gas fluidized beds. *Chem. Eng. Sci.* **1981**, *36*, 327−335.
(42) Darton, R. C.; Lanauze, R. D.; Davidson, J. F.; Harrison, D. Bubble growth due to coalescence in fluidized-beds. *Trans. Inst. Chem. Eng.* **1977**, *55*, 274−280.
(43) Mori, S.; Wen, C. Y. Estimation of bubble diameter in gaseous fluidized beds. *AIChE J.* **1975**, *1*, 109−115.
(44) Clift, R.; Grace, J. R. In *Continuous Bubbling and Slugging*; Davidson, J. F., Clift, R., Harrison, D., Eds.; Academic Press: London, 1985; pp 73−132.
(45) Wilke, C. R. Diffusion properties of multicomponent gases. *Chem. Eng. Prog.* **1950**, *46*, 95−104.
(46) McGee, H. A. *Molecular Engineering*; McGraw−Hill: New York, 1991.
(47) Xu, J.; Froment, G. F. Steam methane reforming, methanation and water-gas shift: I. Intrinsic kinetics. *AIChE J.* **1989**, *35*, 88−96.
(48) Kunii, D.; Levenspiel, O. Bubbling bed model for kinetic processes in fluidized beds -Gas-solid mass and heat transfer and catalytic reactions. *Ind. Eng. Chem. Process Des. Dev.* **1968**, *7*, 481−492.
(49) Kunii, D.; Levenspiel, O. *Fluidization Engineering*, 2nd ed.; Butterworth−Heinemann: Boston, 1991.
(50) Peters, M. H.; Fan, L. S.; Sweeney, T. L. Reactant dynamics in catalytic fluidized bed reactors with flow reversal of gas in the emulsion phase. *Chem. Eng. Sci.* **1982**, *37*, 553−565.
(51) Abanades, J. C. The maximum capture efficiency of CO_2 using a carbonation/calcinations cycles of $CaO/CaCO_3$. *Chem. Eng. J.* **2002**, *90*, 303−306.
(52) Abanades, J. C. Capture of CO_2 from combustion gases in a fluidized bed of CaO. *AIChE J.* **2004**, *50*, 1614−1622.
(53) Alonso, M.; Rodríguez, N.; Grasa, G.; Abanades, J. C. Modelling of a fluidized bed carbonator reactor to capture CO_2 from a combustion flue gas. *Chem. Eng. Sci.* **2009**, *64*, 883−891.
(54) Chen, Y.; Zhao, Y.; Zheng, C.; Zhang, J. Numerical study of hydrogen production via sorption-enhanced steam methane reforming in a fluidized bed reactor at relatively low temperature. *Chem. Eng. Sci.* **2013**, *92*, 67−80.
(55) Florin, N. H.; Harris, A. T. Enhanced hydrogen production from biomass with in situ carbon dioxide capture using calcium oxide sorbents. *Chem. Eng. Sci.* **2008**, *63*, 287−316.